OFFSET DEPENDENCE OF STACKING ATTRIBUTES FOR CRS AND i-CRS OPERATORS

P. Adetokunbo, D. Gajewski, B. Schwarz, and C. Vanelle

email: *peter.adetokunbo@zmaw.de*
keywords: *spread-length bias, wavefield attributes, CRS*

ABSTRACT

Multiparameter stacking operators provide kinematic wavefield attributes to simulate high quality zero offset sections. The quality of these attributes depend on the accuracy of the traveltime moveout used to describe reflection events. The conventional CRS and implicit common reflection surface (i-CRS) stack represent approximations of different accuracy. It has been shown previously that the i-CRS operator provides a better fit to the data than the CRS operator. In this study we quantify the influence of the spread-length bias on the determination of stacking attributes using simple models. For these models it is possible to compare the determined attributes with forward calculated values. The results show that the spread length bias is considerably smaller for the i-CRS operator than for the CRS operator. Therefore, the application of the i-CRS is much more user friendly since the quality of the estimated attributes does not depend on the offset at which they are estimated. It is important to note that the choice of a too short offset compromises the parameter estimation, regardless what operator is used. As a rule of thumb we found that the minimum offset should not be smaller than the half of the target depth.

INTRODUCTION

The CRS and i-CRS stack methods (Müller, 1999; Vanelle et al., 2010; Schwarz, 2011) are techniques which are suited for the simulation of zero-offset sections. Both methods describe the traveltime moveout in offset-midpoint-time domain. The simulation works by means of a coherence analysis using an optimization procedure to estimate kinematic wavefield attributes namely α, R_{NIP} and R_N. In addition, a reliable stacking velocity model can be produced from these attributes.

The CRS method is based on second order, i.e., hyperbolic approximation of the traveltimes whereas the i-CRS formula is of double square root type. Since both operators fit reflection events only approximately the estimated best fit surface does not in general coincide with the observed traveltimes (Müller, 2006). To illustrate this, we apply the coherence analyses with varying search offset apertures to qualitatively and quantitatively investigate the effect of spread-length bias on the estimation of wavefield attributes, the quality of zero-offset simulated stack section and the subsequent post-stack migrated image, where the migration velocity is derived from the wavefield attributes.

METHOD

The CRS operator is a hyperbolic traveltime approximation (Müller, 1999). In mid-point (x_m) and half-offset (h) coordinate the CRS formula (Jager et al., 2001) reads

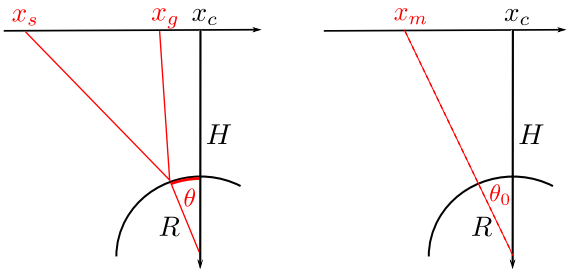

Figure 1: Geometry for the circular reflector (after Schwarz, 2011).

$$t^2(\Delta x_m, h) = (t_0 + \frac{2\sin\alpha}{v_0}\Delta x_m)^2 + \frac{2t_0\cos^2\alpha}{v_0}(\frac{\Delta x_m^2}{R_N} + \frac{h^2}{R_{NIP}}) \quad . \tag{1}$$

where t_0, v_0 are zero-offset traveltime and near surface velocity, respectively, x_0 is the central mid-point location and $\Delta\ x_m = x_m - x_0$ is the mid-point displacement. The quantities R_{NIP}, R_N and α are the kinematic wavefield attributes introduced by Hubral (1983).

The implicit common reflection surface stack, i-CRS, is derived considering a circular reflector with radius R (see Figure 1) in a homogeneous medium centered at (x_c, H). The traveltimes t_s and t_g of the down and up-going ray segments in half-offset and mid-point coordinates are given by

$$t(\Delta x_m, h) = t_s + t_g \quad . \tag{2}$$

where

$$\begin{aligned} t_s^2 &= \frac{(\Delta x_m - h - \Delta x_c - R\sin\theta)^2 + (H - R\cos\theta)^2}{v^2} \quad , \\ t_g^2 &= \frac{(\Delta x_m + h - \Delta x_c - R\sin\theta)^2 + (H - R\cos\theta)^2}{v^2} \quad . \end{aligned}$$

The reflection angle θ that minimizes the traveltime is computed in a recursive manner. For the zero-offset angle θ_0 can be computed analytically providing initial values for t_s and t_g which are used to update θ (Vanelle et al., 2010)

$$\tan\theta = \tan\theta_0 + \frac{h}{H}\frac{t_s - t_g}{t_s + t_g} \quad , \theta_0 = \frac{\Delta x_m - \Delta x_c}{H} \quad .$$

This procedure can be iteratively applied until the desired accuracy is reached. For most applications a single iteration is sufficient. In some special cases (Schwarz, 2011) such as horizontal layering in the subsurface (α=0, $R_N = \infty$) i-CRS reduces to the NMO hyperbola

$$t^2 = t_0^2 + \frac{4h^2}{V_{NMO}^2} \quad . \tag{3}$$

For the case of a diffractor, i.e., R_N=R_{NIP}, the i-CRS operator reduces to the well known double–square–root–equation,

$$t = \sqrt{\frac{t_0^2}{4} + \frac{(\Delta x_m - h)^2}{V_{NMO}^2}} + \sqrt{\frac{t_0^2}{4} + \frac{(\Delta x_m + h)^2}{V_{NMO}^2}} \quad . \tag{4}$$

.

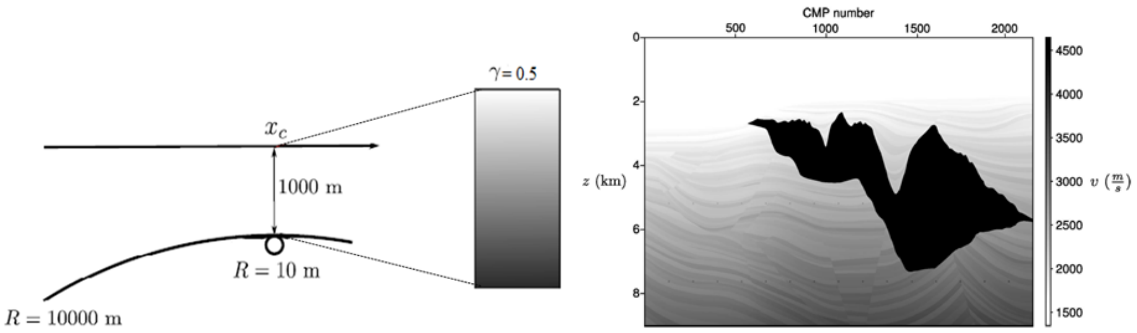

(a) **(b)**

Figure 2: Models considered in this study (a) consists of two different degrees of curvatures representing a limiting diffraction case ($R = 10m$) and a nearly flat reflector ($R = 10.000m$) (Adapted after Schwarz, 2011) (b) Model of the Sigsbee2a dataset.

Table 1: Parameters of the circular reflector datasets.

No. of CMP Bins	Max. CMP Fold	CMP Bin Interval	Min. Half-Offset	Max. Half-Offset	Sampling Interval (ms)
401	81	12.5	0	2000	4

RESULTS

In this section we demonstrate the offset dependence of the CRS and i-CRS operators by considering simple models with interfaces of different curvatures, and complex models. The simple models are beneficial for this study since the traveltimes for this media can be forward calculated analytically which allows a direct comparison with the traveltimes predicted by the CRS and i-CRS operators. Two simple models are considered to investigate whether the spread-length bias is model dependent. The circular reflector is centered in the midpoint aperture, and therefore the normal incident angle is zero. In table 1 we have summarized the acquisition parameters.

Traveltimes

The model (Figure 2) used for this study represents a circular reflector (Schwarz, 2011). The quality of fit of the CRS operators was investigated for two different radii representing very low curvature ($R = 10.000m$, i.e., nearly flat reflector) and the limiting diffraction case ($R = 10$ m). The medium above the curved reflector is a inhomogeneous overburden with a linear vertical velocity gradient $\gamma = 0.5\frac{1}{s}$ and near-surface velocity $v_0 = 2000$ m/s. The wavefield attributes are determined for data with various half offsets. They start from 200 m and are increased in steps of 200 m until a maximum half-offset of 2000 m is reached. To obtain the wavefield attributes the CRS and i-CRS operators are fitted to the reference traveltimes by a three-dimensional optimization minimizing the deviations between the operator traveltimes and the reference traveltimes. The attributes determined in this step are then substituted into the CRS formulas and the corresponding RMS error between operator and reference traveltimes (Figure 3 a and b) is calculated by

$$\delta_{RMS} = \sqrt{\frac{t_i - \widetilde{t_i}}{n}} \quad .$$

where n stands for number of considered combinations of half-offset and midpoint displacement.

The figures show that the i-CRS operator better fits the data since it is located always below the green curve of the CRS operator. Moreover, the gradient with offset of the i-CRS curve is smaller compared to

the gradient of the CRS curves. Particularly for then limiting case of a diffractor the sensitivity of the CRS attribute determination to the offset is very small. These figures display the net effect of the combined application of the wavefield attributes in the CRS and i-CRS traveltime operator. In Figures 3 c-f we compare the offset dependence of individual wavefield attributes. The emergence angle is determined with high accuracy with both operators and the offset dependence is small (note the scale!). For R_{NIP} and R_N we observe that the offset dependence is smaller for i-CRS and we have a deviation between 90 to 300 m where the largest deviations are observed for the largest offset at which R_{NIP} is determined. The determination of wavefield attributes using the CRS operator is more sensitive to offset than with the i-CRS operator. Since in practice we fit traveltime operators to waveforms this case is considered in the following examples.

Waveform Example

The previous section provided inside into the offset behavior of the CRS operators. The direct fitting to traveltimes, however, is not feasible in practice since it requires picking. The fitting of traveltime operators to waveform data is more close to practical applications. The optimization scheme applied here is the CRS implementation by Mann (2002). The underlying numerical experiment is the same as applied to the traveltime example. The difference stems from the fact that the objective function of the stacking procedure maximizes the semblance as an coherence attribute to determine the best fitting stacking parameters. Figures 4 shows the coherence results with a color coded semblance coefficient. The results convincingly show the effect of spread-length bias on the semblance coefficient derived from coherence sections of the CRS and i-CRS implementation. The semblance coefficient gradually decreases with increasing offset (we omit "half" in the following).

For the diffraction case, i.e., the $R = 10$ m model, the i-CRS operator (Fig. 4 a) displays very little spread length bias, i.e., dependence on offset in the semblance analysis. The coherence for the CRS operator (Fig. 4 b) deteriorates very fast with increasing offset . For the model with $R = 10.000$ m the difference with offset between CRS (Fig. 4 c) and i-CRS (Fig. 4 a) are much smaller but still visible at larger offsets.

The wavefield attribute α is determined with high accuracy in both cases (α=0 for this case) and with both operators. The strong variation with offset is an apparent one and caused by the scaling (10^{-4}) of the figure. The wavefield attributes (R_{NIP} and R_N) show a variation with offset which is considerably smaller for the i-CRS operator (about 2-3%) than for the CRS (>15%). The strong gradient of R_{NIP} at short offsets for the CRS operator came as a surprise. Although the traveltime fit is very good for short offsets we observe a very strong sensitivity of this attributes with offset. In other words, a good traveltime fit does not automatically lead to reliable attributes. The i-CRS attributes display a much smaller gradient and the determined values are closer to the forward calculated reference results.

In Fig. 5 we show the percentage deviation of the wavefield attributes with respect to forward computed reference values. Figs. 5a-d show the results for CRS (left) and i-CRS (right) for α (top) and R_{NIP} (bottom) for the 10 m radius. The deviations are generally smaller for i-CRS. An observation already made above for the diffraction case in the examples above. It is interesting to note that the determination of these attributes is unstable for short offsets for both operators despite the fact that the CRS is a short offset approximation. Particularly R_{NIP} is highly overestimated whereas the deviations in the angle are much smaller. To determine the attributes in a reliable fashion we do need move out in our data. The move out at short offsets, however, is too small, i.e., the curvature in the traveltimes is so small that no reliable determination of wave field attributes is possible. Figs. 5e and f display the percentage deviation of for α and R_{NIP} for the 10.000 m model for the i-CRS operator. The deviations of R_{NIP} are considerably smaller in this case as well as the deviations between i-CRS and CRS (not shown here).

Sigsbee2A Data Set

In this section we present some qualitative results using the Sigsbee2A synthetic dataset which represents a typical complex geologic salt setting. In Fig. 6 we present time sections obtained by an operator based post-stack Kirchhoff migration utilizing wavefield attributes which were generated by fitting the i-CRS operator to the data. Tow maximum offsets were considered to determine the wavefield attributes. A short offset of 600 m and a far offset of 4000 m. The poststack migrated sections in Fig. 6 clearly show the

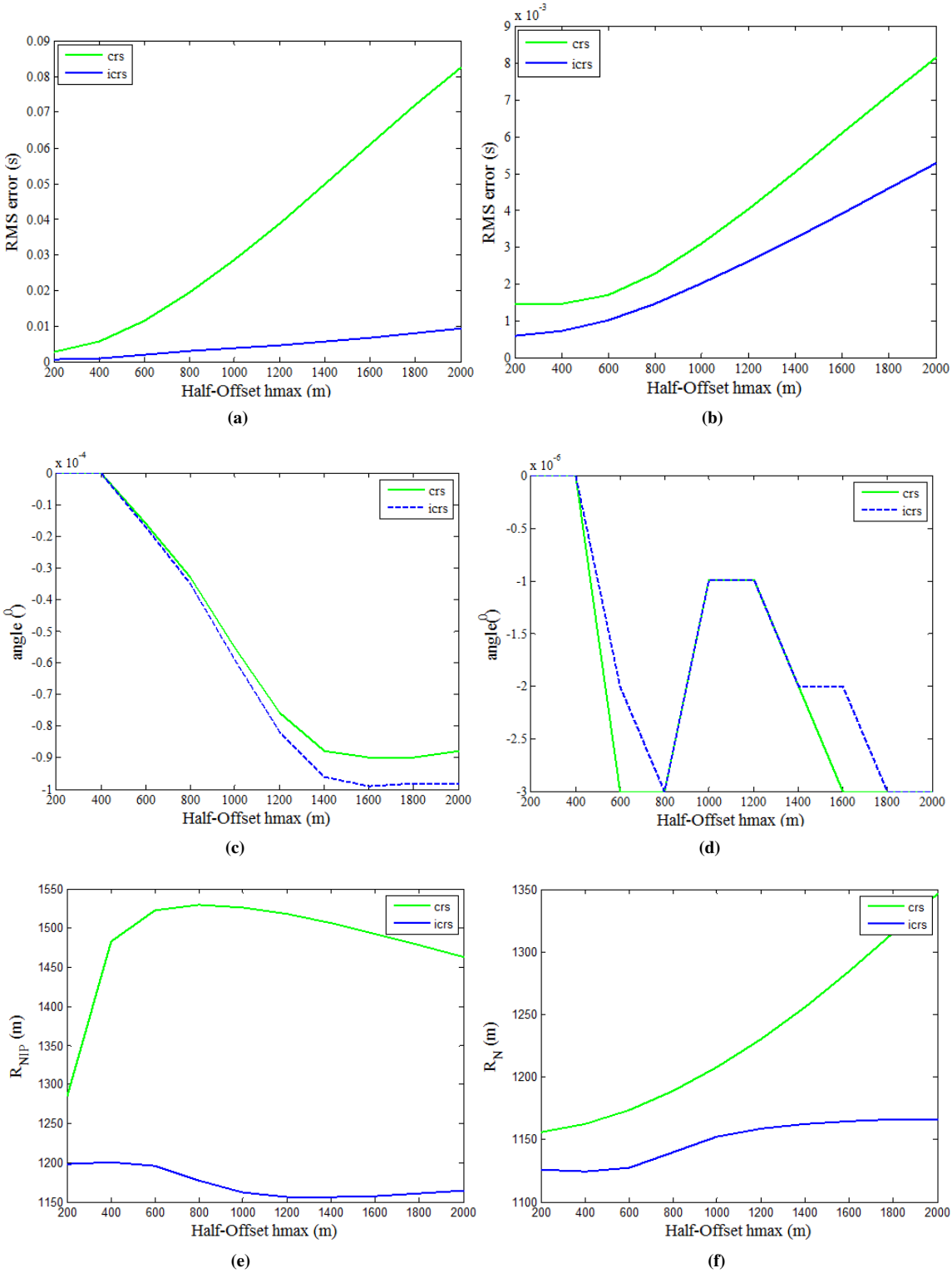

Figure 3: RMS errors of traveltimes and kinematic wavefield attributes as a function of half offset aperture for the two different curvatures: (a) RMS traveltime errors of CRS and i-CRS for $R = 10$ m, (b) RMS traveltime error of CRS and i-CRS for $R = 10.000$ m, emergence angle of CRS and i-CRS for $R = 10$ m (c) and $R = 10000$ m (d), R_{NIP} of CRS and i-CRS for $R = 10$ m (e) R_N of CRS and i-CRS for $R = 10$ m (f).

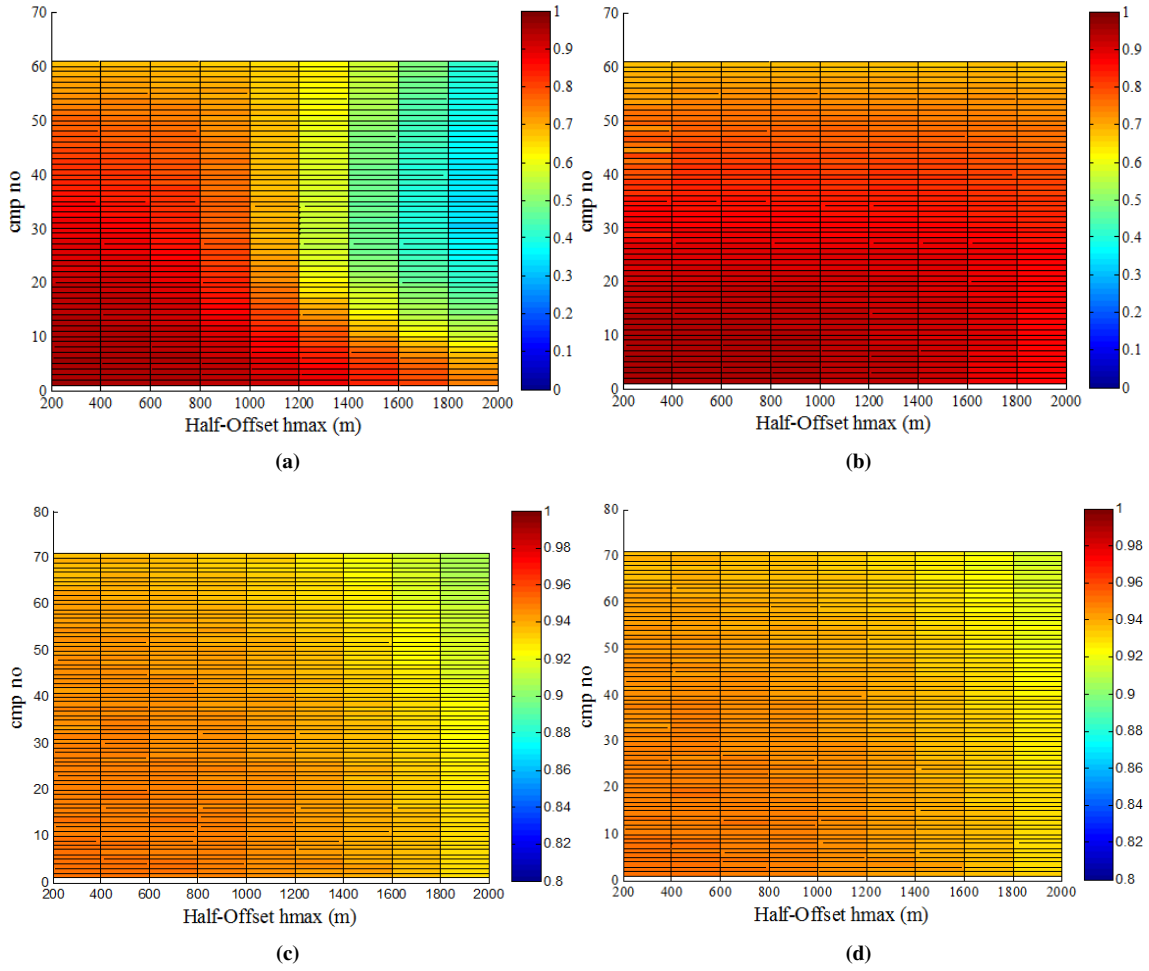

Figure 4: Semblance coefficient plot (a) $R = 10$ m with CRS (b) $R = 10$ m with i-CRS (c) $R = 10.000$ m with CRS (d) $R = 10.000$ m with i-CRS.

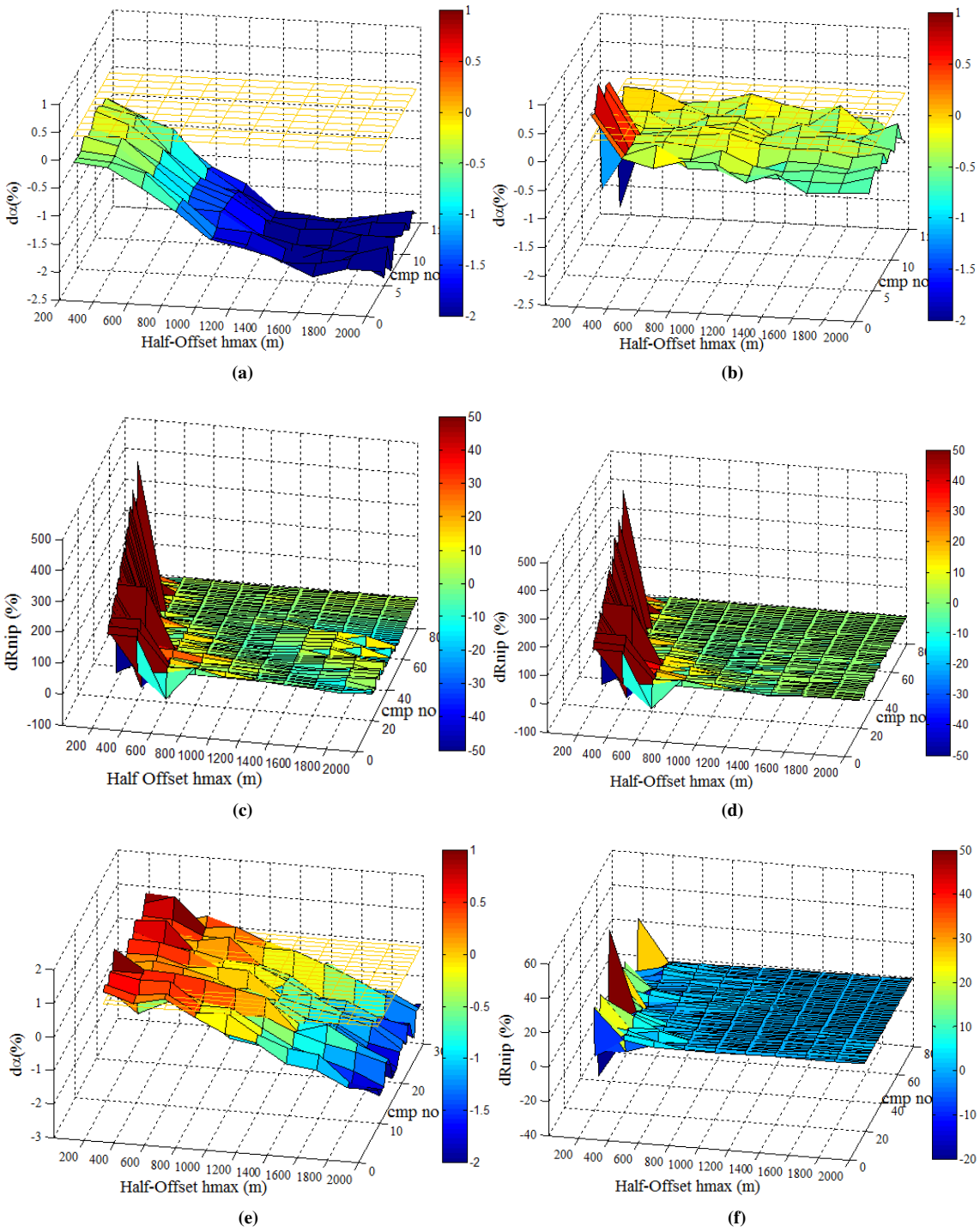

Figure 5: Percentage deviation of kinematic wavefield attributes with respect to forward computed reference values (a) Percentage deviation of emergence angle for $R = 10m$ with CRS (b) Percentage deviation of emergence angle for $R = 10$ m with i-CRS (c) Percentage deviation of R_{NIP} for $R = 10m$ with CRS (d) Percentage deviation of R_{NIP} for $R = 10$ m with i-CRS (e) Typical emergence angle percentage deviation for $R = 10.000m$ (f) Typical R_{NIP} percentage deviation for $R = 10000$ m.

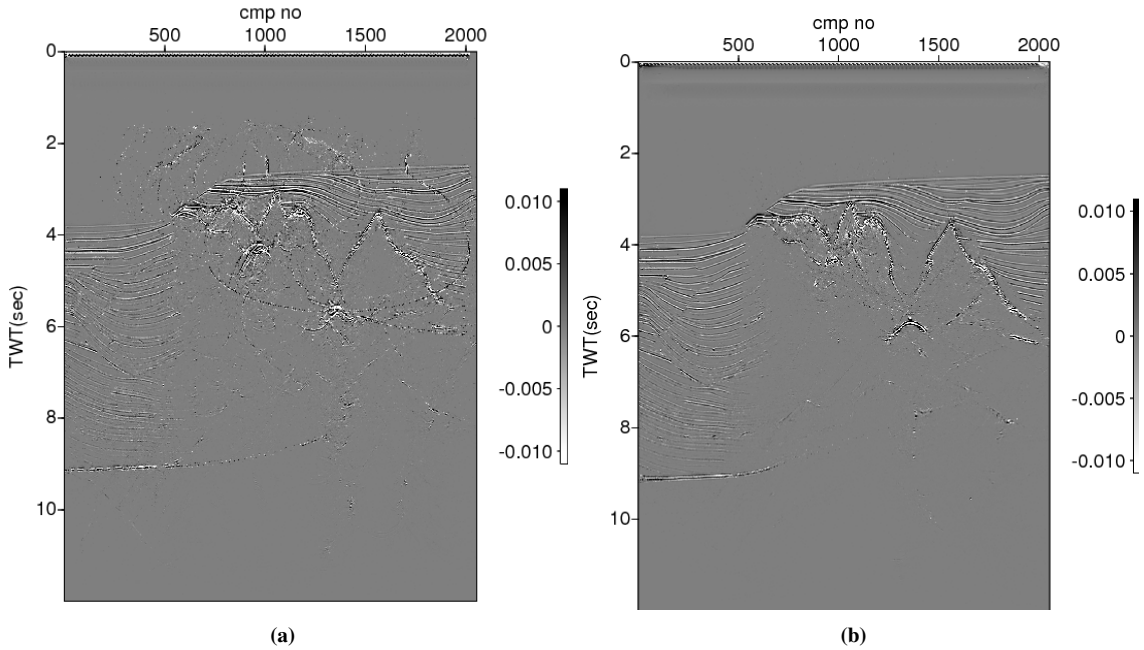

Figure 6: i-CRS operator migrated section utilizing (a) 600 m, and (b) 4000 m maximum offset for wavefield attribute determination.

overall effect of spread-length bias on the quality of attributes. At 600 m offset apertures, events are not properly located and the image is distorted. At 4000 m the i-CRS operator produces a good description of the model. This confirms the previous observation that the stability of the attributes is unstable for too short apertures. Unreliable attributes will compromise subsequent processing steps utilizing them.

DISCUSSION

The i-CRS operator provides better estimates of the wavefield attributes compared to the CRS operator and shows a considerably smaller spread length bias. In other words: The determination of wavefield attributes is much less sensitive to the maximum offset of the fitting aperture at which they are determined. This is a user-friendly feature. The advantage particularly applies to the diffraction case. The i-CRS better accounts for R_{NIP} and R_N especially at larger offsets in this case. Since diffraction amplitudes are usually very small this feature is an advantage for diffraction imaging since coherent energy can be collected for more traces increasing the stack amplitude.

The results of the synthetic data convincingly show the effect of spread-length bias on the semblance coefficient derived from coherence sections of the i-CRS implementation. In both considered model situations (almost flat reflector and diffraction limit), the semblance coefficient gradually decreases with increasing offset. For the case of the diffractor, the difference in operator performance between CRS and i-CRS is significant as the semblance coefficient decreases with higher half offset for CRS but is generally very stable for i-CRS. The determined wavefield attributes R_{NIP} and α are generally not stable with increasing spread length for the CRS. Deviations of more than 20% are observed for R_{NIP} with a strong variation with offset, i.e., a strong spread length bias, at short offsets. This is a somewhat surprising feature since the hyperbolic CRS operator is a short spread approximation.

The i-CRS shows a much smaller spread length bias and leads to good estimates of the wavefield attributes even at large offsets. The good fit at large offsets may not be exploitable in the presence of strong lateral velocity variations. Since modern exploration targets usually are in complex geological environments this favorable offset behavior of the i-CRS operator may be of limited practical relevance.

CONCLUSIONS

We have presented the influence of the spread-length bias of the CRS and i-CRS stacking operators. We investigated and quantified the spread length bias using simple models of an almost flat reflector (zero curvature) as well as the limiting diffraction case (infinite curvature). For this models wavefield attributes could be forward calculated and compared to the determined attributes using the CRS and i-CRS operator. For a qualitative comparison we used the complex Sigsbee 2a dataset. As has been previously shown the i-CRS operator has a superior fit to the data when compared to the CRS operator. In addition, also the spread length bias of the i-CRS is considerably smaller which makes the application of this operator much more user friendly. The choice at which offset the wavefield attributes are estimated is less critical for the i-CRS operator than for the CRS operator. The better estimation of the wavefield attributes will benefit all subsequent processing steps using these.

It is also important to note that a too short spread will compromise the determination of attributes in any case, regardless what operator is used. The results for the simple models considered in this study we could suggest as a rule of thumb that the offset should not be smaller than half the target depth. Future work may include the correction of offset dependence in the i-CRS implementation to improve the performance of stacking and wavefield parameter estimation.

ACKNOWLEDGEMENTS

The authors thank the members of the Applied Seismic Group, University of Hamburg, for helpful discussions. This work is partially supported by King Fahd University of Petroleum and Minerals (KFUPM), Saudi Arabia.

REFERENCES

Hubral, P. (1983). Computing true amplitude reflections in a laterally inhomogeneous earth. *Geophysics*, 48:1051–1062.

Jager, R., Mann, J., and Hubral, P. (2001). Common reflection surface stack: Image and attributes. *Geophysics*, 66:97–109.

Mann, J. (2002). *Extensions and applications of the common reflection surface stack method*. PhD thesis, University of Karlsruhe.

Müller, N. (2006). Elimination of the spread-length bias in the common reflection surface stack. In *SEG/New Orleans 2006 Annual Meeting*.

Müller, T. (1999). *The Common Reflection Surface stack method – seismic imaging without explicit knowledge of the velocity model*. PhD thesis, University of Karlsruhe.

Schwarz, B. (2011). A new nonhyperbolic multi-parameter stacking operator. Master's thesis, University of Hamburg.

Vanelle, C., Kashtan, B., Dell, S., and Gajewski, D. (2010). A new stacking operator for curved subsurface structures. In *SEG 80th Annual Meeting, Expanded Abstracts*.